

DYNAMICS OF TWO COUPLED ROTATORS KICKED WITH DELAY — A MODEL FOR CARDIORESPIRATORY SYNCHRONIZATION*

TEODOR BUCHNER

Physics of Complex Systems Division, Faculty of Physics
Warsaw University of Technology
Koszykowa 75, 00-662 Warsaw, Poland

(Received April 19, 2010)

A model of cardiorespiratory synchronization, *i.e.* the synchronization between the heart rate and the breathing rate, is proposed. From a mathematical point of view it is a delayed nonlinear system — a pair of pulse coupled rotators. The model is studied theoretically and numerically. Classification of synchronization states is supplied by theoretical analysis and verified by numerical experiment. The constitutive role of phase resetting and refraction in synchronization is discussed. As the model is minimalistic it is discussed how well can it mimic the original physiological phenomena.

PACS numbers: 05.45.-a, 05.45.Xt

1. Introduction

In a living organism, such as a human body, there exists a great variety of complex biological rhythms [1]. They govern various aspects of biological life in order to maintain *homeostasis*: the state of optimum internal conditions against external forces. On the other hand the *homeostasis* is a result of a compromise between different regulatory feedback loops active within the human body.

Probably the most important example of a cooperative behavior is the phenomenon of cardiorespiratory synchronization (CRS) [9]: the synchronization between the heart rhythm and the breathing rhythm. These two separate vital rhythms having different generators do not compete but synchronize with each other to optimize the cardiorespiratory dynamics.

* Presented at the XXII Marian Smoluchowski Symposium on Statistical Physics, Zakopane, Poland, September 12–17, 2009.

In physical terms the phenomenon of CRS may be described as either phase synchronization or frequency synchronization. By formal definition two systems described by phases Φ and φ are in the state of frequency synchronization if for any values of integer parameters n and m the following relation is fulfilled.

$$|n\Phi(t) - m\varphi(t)| < \text{const.} \quad (1)$$

Equation (1) requires that for some integers n and m the phase difference is bounded, although the difference in phases may be the function of time. Therefore, in such a state two phases are not guaranteed to have the same difference at any instant in time. State of phase synchronization, also known as phase locking or phase entrainment, is obtained if:

$$|n\Phi(t) - m\varphi(t)| = \text{const.} \quad (2)$$

In such a state one of phases strictly follows the other one with some constant phase shift. For some systems the condition defined by Eq. (2) cannot be reached: see *e.g.* [24]. In such cases equation (1) is used as definition of phase locking. In well trained athletes, in infants and in normal subjects during sleep, regions of phase synchronization between breathing and heart rate occur: most often 3:1 (three heartbeats per single breath) and 5:2 [9].

One problem which is often considered in regards to the CRS is the directionality of the coupling. There are many papers in physiological and cardiological literature treating the heart rhythm as subordinate to the breathing rhythm [4, 8]. It is a well known fact that the respiratory-related activity of efferent cardiac vagal nerves has a strong influence both on the mean value of the heart rate [2] and on its standard deviation [3]. This coupling introduces the Respiratory Sinus Arrhythmia (RSA): a sinusoidal frequency modulation of the heart rate [4, 8]. Various aspects of the CRS, including experimental methods to measure the directionality of the coupling are summarized in the review paper [10].

The fact that is not so widely acknowledged is that breathing has also a vivid response to the blood pressure and its oxygenation. The breathing rate is as sensitive to the heart rate as the heart rate is to breathing [14–16]. More importantly, this response is phase-sensitive: it depends on the instantaneous phase of the respiratory rhythm [15].

There seems to exist experimental evidence [7] based on statistical physics approach [13] that the coupling is not only bidirectional, but that there is no clear dominance of any of the rhythms and each of them seems to be far from its intrinsic frequency.

1.1. Models of cardiorespiratory synchronization

The experimental findings described above have their counterpart in the modelling. The relation between the rhythms has been modelled using two approaches.

In the first approach relation between the rhythms is described in terms of phases. Both rhythms [20] or only one of them [15] are represented by a phase variable which is either described by the ordinary differential equation [20] or by the *integrate and fire* type of dynamics [15]. As the output has a form of the spike train (with spikes at the moments of heart beats: *i.e.* when the phase exceeds 2π) such a system may be considered a point process. In these models the dominant direction of the coupling is either from the heart to breathing [15] or the opposite [20], although the theoretical framework is symmetric with respect to the direction of the coupling [20]. The integrate and fire model [15] was also converted to a discrete map [11]. Still, however, the coupling considered in this model is unidirectional. Probably following the method used in chronobiology [22] the authors try to introduce the RSA by introducing a modulation of the firing threshold. This, however, does not have a direct physiological bearing. The integrate and fire approach is also used in another model of RSA [5] where an input to the integrate and fire model is an Ornstein–Uhlenbeck process.

The second approach is to construct an integrative physiological model which describes many physiological variables, such as blood pressure, heart rate and neural activities [23]. The dominating direction considered there is from breathing to the heart. The other direction is also included but the relation is much weaker.

The main finding in both approaches is the presence of the Arnol'd tongues in which both rhythms are phase synchronized. We were able to show the same result using a simplification of the second approach where the natural heart pacemaker, the sinus node, was represented by the modified van der Pol relaxation oscillator [6].

A direct motivation for current work was the finding that in physiological conditions both rhythms are coupled and their mean frequencies are far away from their intrinsic frequencies [7]. Due to this, both rhythms show a tendency to escape towards their intrinsic frequency. A natural consequence of such a finding is to build up a basic model which would have such a feature. The method we used was to express the model [15] in terms of phase dynamics [20, 24] and generalize it. Another aim was to introduce bidimensional coupling in such a way that the RSA could appear in the model as a result of coupling which seems to be more physiologically relevant. We also kept in mind that the model should (a) serve as a generic example of mutually coupled rotators and (b) be as simple as possible to enable analytical analysis.

The paper is organized as follows: Section 2 introduces the model of dynamics of two mutually coupled rotators delta-kicked with delay which serves as a generalized model of the CRS. Section 3 summarizes the analytical results: derivation of the condition for synchronization (3.1) and calculation of the phase response curve (PRC) (3.2) which is important for determination of the stability of the synchronization regions. The analytical findings are supported by the numerical experiment described in Section 4, in which the phase diagram of the system is obtained, together with synchrograms and interspike interval plots that describe individual dynamical states. Finally, the results are widely discussed (Section 5) and conclusions are drawn (Section 6).

2. The model

The model equations define the dynamics of two phases:

$$\dot{\varphi} = r + m\delta(t - t_j - \tau_1) , \quad (3)$$

$$\dot{\Phi} = R + M\delta(t - t_i - \tau_2) . \quad (4)$$

Physiological interpretation would be such that φ denotes the phase of the heart rhythm, whereas Φ the phase of the breathing rhythm. Both phases are in $1/(2\pi)$ units so that phase difference 1 is equal to full rotation. Parameters r and R define the angular velocity of each of rotators. As the motivation for introducing such a system comes from physiology, we will assume $r > R$. The ratio of velocities will be defined as:

$$\omega = \frac{r}{R} . \quad (5)$$

Here $\omega = 8$ is used, as approximately such is the ratio of frequencies of uncoupled breathing and uncoupled heart rate [7]. Therefore, the rotator defined by Eq. (3) is referred to as fast, whereas the one defined by Eq. (4) as slow. Phases of the fast and the slow rotator taken modulo 1 are denoted by $\tilde{\varphi}$ and $\tilde{\Phi}$, respectively.

The definition of firing times t_i and t_j is the following:

$$t_i : \varphi(t_i) = i , \quad (6)$$

$$t_j : \Phi(t_j) = j . \quad (7)$$

Equations (6) and (7) define moments in time when a full cycle is complete (relevant to “fire” in *integrate and fire* models or “spiking” in neural models). This corresponds to an integer value of each of phases.

Both rotators are pulse-coupled: at certain delay after one of rotator “fires” the other rotator is kicked by a delta pulse. Due to the delay, the “fire” (cause) and the phase advance (effect) are separated in time. In specific conditions the cause and the effect may belong to different cycles, as discussed below. Parameters m and M define the height of the delta kick (pulse), which appears at time τ_1 for the first rotator and τ_2 for the second rotator, after the other rotator has fired (t_j and t_i , respectively).

The model is generic: taken directly it describes the dynamics of two mutually coupled overdamped oscillators. The list of resemblances is, however, longer, including the standard map [17], the circle map-based cardiac oscillator [18,19] and the pulse-coupled oscillators intensively studied in neuroscience [12].

An example of the model output is shown in Fig. 1. Note the discontinuities of phase at the moments in time in which the rotator has been kicked.

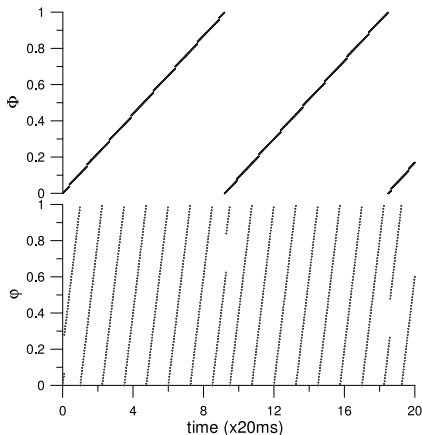


Fig. 1. Example output from the model for parameters. The discontinuities of both curves occurring at phase smaller than 1 are caused by kicks and are located at respective delay after the other rotator “fires”.

2.1. Variant of the model

During the analysis of the model features one important modification has been made. From Eq. (3) and (4) it comes that due to the kick the phase may exceed 1. In such a case nothing particular happens as $\varphi(t)$ is just growing continuously to infinity. For the reasons explained in subsequent chapters it occurred necessary to disallow such a situation and, when $\tilde{\varphi} > 1$ or $\tilde{\Psi} > 1$, reset the respective phase to the integer value. Mathematically it may be expressed by turning the respective kick height into a function:

$$m(\varphi) = \begin{cases} m & \text{for } m + \varphi \leq 1, \\ m + \varphi - 1 & \text{otherwise,} \end{cases} \quad (8)$$

and respectively for M :

$$M(\Phi) = \begin{cases} M & \text{for } M + \Phi \leq 1, \\ M + \Phi - 1 & \text{otherwise.} \end{cases} \quad (9)$$

3. Theoretical results

Theoretical analysis determines the location and properties of synchronization regions in the parameter space. The stability may be determined from the analytic form of the phase response curve (PRC). The stability of the fixed points of the PRC determines the existence of Arnol'd tongues. In this chapter an unmodified version of the model is used: *i.e.* without the modifications defined by Eqs. (8) and (9).

3.1. Synchronization regions

We would like to calculate parameter values at which phase synchronization $n : m$ may be obtained. Calculations below are led for the simplest case: $1 : k$, but the argumentation may be easily extended to cover any $n : m$ case which is explained at the end of this section. First, we introduce a Poincaré section at a hyperplane defined by the condition $\tilde{\Phi} = 0$. The period in time between consecutive crossings of this section will be referred to as cycle of $\tilde{\Phi}$. The ordinal number of a cycle is denoted as n . Next we introduce an integer winding number:

$$k = \left[\lim_{t \rightarrow \infty} \frac{\varphi(t)}{\tilde{\Phi}(t)} \right]. \quad (10)$$

Here the square brackets denote the integer part: *i.e.* the highest integer not greater than. From Eqs. (3), (4) and (5) it follows that, in the absence of kicks, the value of k satisfies $0 < k \leq \omega$ as such is the increment of phase φ during one cycle of $\tilde{\Phi}$.

Let us assume that the $n + 1$ -th cycle of $\tilde{\Phi}$ begins at the time t_0 , with $\tilde{\Phi} = 0$ and ends at $t_0 + \Delta t$ when the next crossing of the Poincaré section takes place. As the time Δt corresponds to one full cycle of a slow rotator, therefore the phase of this rotator by definition increments by 1. The phase of the fast rotator at the beginning of a cycle is $\varphi = \varphi_n$ and at the end of a cycle: φ_{n+1} . Let us now analyze the phase increments. The phase increases due to the angular velocity and due to kicks. Integration of the angular velocity terms gives phase increment equal to $r\Delta t$ and $R\Delta t$, respectively. The “kick” part depends on the number of kicks each rotator obtains during

the full cycle of $\tilde{\Phi}$. For simplicity we assume that the last: M -th kick does not cause significant phase overshoot, characterized by $\tilde{\Phi} > 1$, for the slow rotator and the total increment of $\tilde{\Phi}$ during one cycle is exactly 1. This assumption is justified by the quality of the approximation.

During the whole cycle of $\tilde{\Phi}$ the fast rotator obtains only one kick: at delay τ_2 , *i.e.* at physical time $t_0 + \tau_2$. For simplicity we assume that $\tau_2 < 1/R$ so that the kick always acts in the cycle of $\tilde{\Phi}$ following time t_0 when it was caused, although in a synchronized state this is irrelevant. During full cycle of $\tilde{\Phi}$ the fast rotator will make k full cycles plus a normalized phase increment which may be denoted as ε_n . In a synchronized state, φ has to advance exactly by k , hence the normalized phase increment ε_n vanishes. This property of ε_n makes it useful for numerical detection of phase synchronization — as described in Section 4. Therefore, the phase increment of a fast rotator during $n + 1$ -th cycle may be expressed as:

$$\Delta\varphi = \varphi_{n+1} - \varphi_n = k + \varepsilon_n = r\Delta t + m. \tag{11}$$

During a full cycle of $\tilde{\Phi}$ the slow rotator obtains k kicks that advance its phase by kM . Total phase increment of the slow rotator is given by:

$$R\Delta t + Mk = 1. \tag{12}$$

As already mentioned, we assume that the single kick occurs not later than $t_0 + (1 - M)/R$ so that the phase will not “overshoot” 1. Note only, that in case of overshoot the equation (12) overestimates Δt by at most M/R : the overshoot means that the phase advance related with kicks is between $(k - 1)M$ and kM .

Combining (12) and (11) we reduce the unknown variable Δt and the phase increment of the fast rotator may be expressed as follows:

$$\Delta\varphi = \omega(1 - Mk) + m. \tag{13}$$

Following Eq. (11) the condition for synchronization is $\varepsilon_n = 0$ which gives $\Delta\varphi = k$. Introducing this into (13) gives the synchronization condition in the form:

$$M_k = \frac{\omega - k + m}{\omega k}. \tag{14}$$

The above condition defines the synchronization regime: *i.e.* the value of M_k at which the integer winding number is equal to k . The accuracy of Eq. (14) is discussed in Section 4.

If we define as cycle a period of time between every m -th crossing of the Poincaré section, we may find regions of synchronization of type $m : k$ using the method described above.

3.2. Phase response curve

Phase response curve (PRC), following the notation used here, will be the function of the normalized phase $\tilde{\varphi}_n$. For the n -th iteration its value is equal to ε_n : the normalized phase increment during the full cycle of $\tilde{\Phi}$. In this chapter the PRC will be denoted $f(\tilde{\varphi})$ to point out that it is not related to any specific iteration n .

In order to find the PRC we have to determine the sequence of events during a full cycle of $\tilde{\Phi}$. Depending on the values of angular velocities, pulse height and delay times, different events in each of rotators may appear in different sequence and at different moments in time. Such a sequence for typical parameter values is summarized in Table I. The initial condition for both rotators at the beginning of the cycle is $(\varphi_n, \tilde{\Phi}_n) = (\varphi_0, \Phi_0)$. The initial phase of the slow rotator is $\Phi_0 = 0$, however if there is any “pending” kick

TABLE I

Single cycle of evolution of the model. Parameters R, M and τ_2 represent the angular velocity, the height and the delay of the kick for the slow rotator, whereas parameters r, m and τ_1 represent the same parameters for the fast rotator. Initial condition for the cycle is given by (φ_0, Φ_0) . The amount of physical time corresponding to the full cycle of $\tilde{\Phi}$ is labeled as t_k in the bottom rows of the first column. The phase of the fast rotator at the end of the cycle is denoted by $\tilde{\varphi}_{n+1}$ in the bottom rows of the right column. Symbol ^F denotes “fire” of a certain rotator and the star * means that the rotator was given a kick. Symbols ^A and ^B denote two scenarios of the phase evolution. For brevity we use such a convention that if the symbol t appears in the $\tilde{\Phi}$ column, the corresponding time (*i.e.* the value from the “Time” column) should be substituted instead.

Time t	Phase $\tilde{\Phi}$	Phase $\tilde{\varphi}$
0	Φ_0	$\tilde{\varphi}_n = \varphi_0$
$\frac{(1-\varphi_0)}{r}$	$\Phi_0 + Rt$	1 ^F
$\frac{(1-\varphi_0)}{r} + \tau_2$	$\Phi_0 + Rt + M^*$	$r\tau_2$
$\frac{(1-\varphi_0)}{r} + \tau_2 + \tau_1$	$\Phi_0 + Rt + M$	$r\tau_2 + m^*$
$\frac{(2-\varphi_0)}{r} - \frac{1}{m}$	$\Phi_0 + Rt + M$	1 ^F
$\frac{(2-\varphi_0)}{r} - \frac{1}{m} + \tau_2$	$\Phi_0 + Rt + 2M^*$	$r\tau_2$

... here come last 2 steps repeated $(k - 3)$ -times

$$\frac{(k-\varphi_0)}{r} - \frac{1}{m} + \tau_2 \rightarrow t_k \quad \left| \quad \Phi_0 + Rt_k + kM^* > 1^F \quad \right| \quad r\tau_2 \rightarrow \tilde{\varphi}_{n+1} \quad A$$

Alternatively, if $\Phi_0 + Rt_k + kM < 1$

$$\frac{1-kM-\Phi_0}{R} \rightarrow t_k \quad \left| \quad \Phi_0 + Rt_k + kM = 1^F \quad \right| \quad \omega(1-kM-\Phi_0) \rightarrow \tilde{\varphi}_{n+1} \quad B$$

caused in the previous cycle its effect may be easily introduced by setting $\Phi_0 = M$. The presence of such pending kicks comes from the presence of the delay τ_2 , which introduces the delay between a cause (“fire” of the fast rotator in previous cycle) and the effect (the slow rotator given a kick in current cycle).

From the last column the value of the phase $\tilde{\varphi}_{n+1}$ at the end of the cycle may be read. By subtracting from it the initial phase φ_0 we calculate the phase response curve (PRC). Following [12] we may treat the PRC as a map function which defines the evolution of the $\tilde{\varphi}_n$ on the surface of the Poincaré section hyperplane between consecutive cycles.

Note that this end-cycle phase value does not directly depend on the parameter m . As the phase φ is reset many times before the cycle is completed, it results only in shifting the time by $1/m$. There are two alternative scenarios of the phase evolution at the end of cycle that are denoted A and B . If the condition $\tilde{\Phi} >= 1$ is met during the k -th kick, *i.e.* at time τ_2 after the fast rotator has fired, the final phase of the fast rotator is $\tilde{\varphi}_{n+1} = r\tau_2$. This leads to the phase response curve which is linear in $\tilde{\varphi}$ and decreases monotonously:

$$f_A(\tilde{\varphi}) = r\tau_2 - \tilde{\varphi}. \tag{15}$$

Scenario B is shown in the last row of the table: when the phase Φ reaches 1 by its own evolution (with angular frequency R). Then, the final phase is equal to the initial phase plus the total phase increment during the cycle. This gives the PRC in form:

$$f_B(\tilde{\varphi}) = m + \omega(1 - \Phi_0) - k(1 + \omega M). \tag{16}$$

Note that in scenario B the PRC does not explicitly depend on φ_0 . The indirect relation is through the parameter $\tilde{\Phi}_0$ which will be discussed below. Regardless of the value of k and of the value of $\tilde{\varphi}$ the PRC for variant B is always piecewise constant as a function of $\tilde{\varphi}$.

An example of the PRC is shown in Fig. 2. In the whole range of $\tilde{\varphi}$ there may appear scenario A (part c), B (part (a)) or both of them (part (b)). Plots for $k = 2$ and $k = 3$ (not shown) are piecewise constant — similar to the one for $k = 1$. The first qualitative change appears at $k = 4$ where the mixed evolution scenario appears. Above $k = 4$ the scenario is always A and the corresponding PRC does not depend on k . The point of discontinuity corresponds to the value $\tilde{\varphi}_M = r\tau_2$. For $\tilde{\varphi} < \tilde{\varphi}_M$ there is a “pending kick” from the previous cycle which is taken into account by setting $\Phi_0 = M$ in Eq. (16).

Determination of fixed points of the PRC is straightforward: for scenario A we readily obtain from Eq. (15) and Fig. 2 (c) that the fixed points are located at: $\tilde{\varphi}_{A,1}^* = 1/2 r\tau_2$ and $\tilde{\varphi}_{A,2}^* = 1/2 (r\tau_2 - 1)$. In scenario B , the

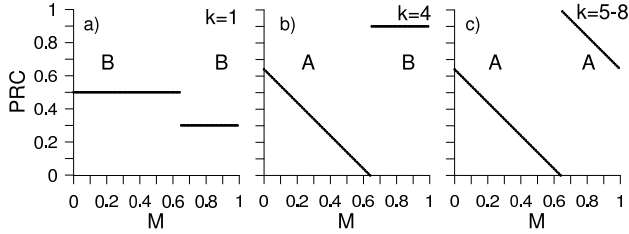


Fig. 2. Example of the phase response curve $f(\tilde{\varphi}_n)$ which governs the evolution of the phase $\tilde{\varphi}_n$ *i.e.* on the surface of the Poincaré section for different values of the winding number k . Part (a) shows the PRC for $k = 1$, part (b) for $k = 4$ and part (c) for $k = 5, 6, 7, 8$. The values of other parameters used for this calculation are $R = 0.2$, $\omega = 8$, $m = M = 0.1$, $\tau_1 = 0.1$, $\tau_2 = 0.4$. Regions in which scenario B or A appears are marked accordingly.

locus of the fixed point depends on the piece of the piecewise constant curve which intersects with the diagonal. Actual locus of this point is, however, not important for further analysis.

Concerning the stability of these fixed points, we can see that in scenario A the slope of the PRC is (-1) everywhere, which means that the stability is marginal and each initial condition different from any of $\tilde{\varphi}_A^*$ will lead to stable orbit of period 2. In scenario B the slope is nearly everywhere 0 so each initial condition, under action of the map defined by the PRC, will be attracted to the stable fixed point $\tilde{\varphi}_B^*$. Neither of points is repelling. According to [12] (Subsection 2.4 thereof) synchronization takes place (and Arnol'd tongues appear) only if a fixed point is repelling and $\tilde{\varphi}$ evolves to 0 or 1 *i.e.* falls into the synchronized state. Inverting the argumentation from [12], in our case when the fixed points are at least marginally stable, the system is never driven to synchrony.

Introduction of the modifications defined by Eq. (8) and (9) affects the PRC in such a way that values of m and M that appear in Eq. (16) become functions of the corresponding phases which introduces conditions for synchronization.

The above analysis enabled us to determine the loci of synchronization regions in the parameter space. The regions of synchronization for the non-modified case have measure 0 in parameter space and no synchronization regimes equivalent to Arnol'd tongues are observed [12].

4. Numerical results

The model was implemented numerically in order to verify the analytical results. Numerical procedure used Runge–Kutta method of the order of 4 with fixed time step equal 20 ms. The delta-kick was not integrated

but was added to the output of the Runge–Kutta method. Below we use two convenient techniques of visualization of synchronization states. In the synchrogram technique [9, 20] we mark along the vertical axis the values of phase of one (primary) rotator (usually the slower) at the moments when the second (secondary) rotator “fires”. Values of phase from one cycle of the slow rotator form a set of points along the vertical axis. The horizontal axis is scaled in cycles of the primary rotator. The second method is to plot time intervals between moments when the rotator “fires”. Such a plot is widely used in neural dynamics, where it is referred to as interspike intervals (ISI) plot: intervals between spikes of a single neuron. Such a name will be adopted here. An example of both plots is shown in Fig. 3 for two different dynamical states. Part (a) and (b) show synchrograms. Part (c) and (d) show the ISI of the slow rotator. Part (e) and (f) show the ISI of the fast rotator. Parts (a), (c) and (e) show the synchrogram and the ISI plots for an unsynchronized state obtained for the unmodified model. Parts (b), (d) and (f) show the synchrogram and the ISI plots for a synchronized state obtained for the modified model.

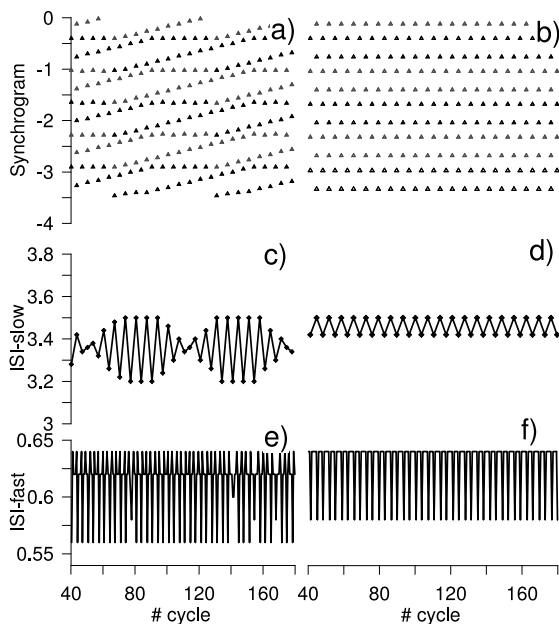


Fig. 3. Example of synchrograms and ISI plots for unmodified (left column) and modified (right column) model. Unmodified model is in a non-synchronized state. Modified model is in a synchronized state. Parts (a) and (b) show synchrograms. Parts (c) and (d) show the ISI of the slow rotator. Parts (e) and (f) show the ISI of the fast rotator. Parameters of both models are: $m = 0.1, M = 0.06, R = 0.2, \omega = 2, \tau_1 = 0.1, \tau_2 = 0.4$.

4.1. Phase diagram

Figure 4 shows phase diagrams in variables M and m : without (a) and with (b) phase resetting. The regions of synchronization are marked by the gray area. It may be seen that for the system without resetting the regions of synchronization are sparse and very narrow. It may be seen, however, that the synchronization regions are located along the lines of $M_k(m)$ — as predicted by Eq. (14). This pretty good accuracy seems to justify the approximations done during derivation of Eq. (14). It may also be seen that for the system with phase resetting, the synchronization areas are wide. Note also the discontinuity of the synchronization regions near $m = 0.4$. It probably corresponds to the value of $\tau_2 = 0.4$ used in calculations, although the corresponding scenarios were not analysed in depth (like the scenarios A and B described in chapter 3.2). The synchronization was detected using a criterion based on the standard deviation of period of the slow oscillator: in synchronized states this values were by 10 orders of magnitude lower, as compared to the non-synchronized states. No other synchronization index that we have used did show such an accuracy. We have used all the indices described in [20] but the detailed description of these results is rather a separate topic and will be published elsewhere.

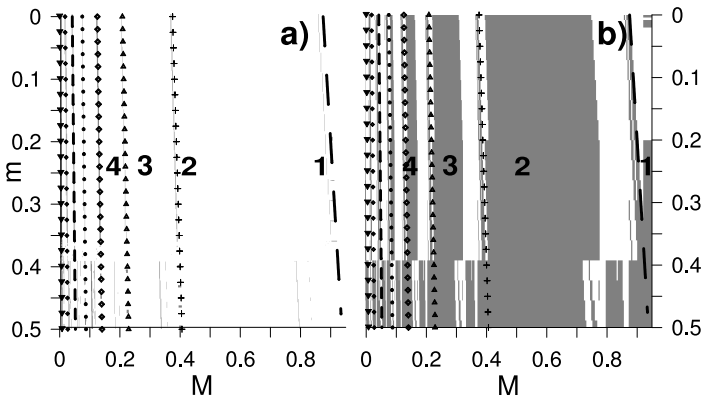


Fig. 4. Phase diagram of the system in variables M and m . Part (a) shows phase diagram of the unmodified system (without phase resetting), whereas part (b) shows phase diagram of the system with phase resetting. The regions of synchronization are marked as gray area. Numeric values correspond to the winding number k in corresponding area. The vertical lines in both parts show the loci of synchronization regions as defined by Eq. (14) for different values of the parameter k . First line on the right (long dash) corresponds to $k = 1$, the second (crosses) to $k = 2$, the third (triangles) to $k = 3$. Next lines correspond to $k = 4, 5, 6, 7$ and 8 .

5. Discussion

Despite its simplicity, the model exhibits many different dynamical states. In the parameter space of the unmodified model the strongest synchronization that may be achieved is frequency locking [20]. In this state ε_n has some constant (or nearly constant) value, either positive or negative, *c.f.* Eq. (11)). The synchrogram of such a state shows that within one cycle the values of phase $\tilde{\Phi}$ remain at constant distances but the sum of phase differences is either larger than 1 (and the lines on the synchrogram are directed upwards) or smaller than 1 (and the lines are directed downwards).

5.1. Nearly-synchronized and non-synchronized states

Apart from frequency locking there may appear also different nearly-synchronized states. One interesting example is a state in which the ISI of the slow rotator exhibit modulation with two apparently incommensurate frequencies: fast “carrier” frequency and slow “envelope” frequency: Fig. 3 (c). The corresponding ISI of the fast rotator seem to be quasiperiodic or chaotic: Fig. 3 (e). The synchrogram of this case shows a pattern of intersecting horizontal and slanted lines: Fig. 3 (a). Note that the power spectrum for the ISI of the slow rotator would show two peaks, despite the fact that the rotator is driven only by one system: the fast rotator. Introduction of the second frequency comes from the fact that the coupling between both rotators is bidirectional. This might possibly be the mechanism of introduction of the low frequency oscillations observed in the heart rate, the blood pressure variability, as well as in the power spectrum of the breathing rhythm. The origin of these oscillations is not yet fully understood, despite many hypotheses that have been formulated [21].

When the values of M and m are far from the synchronization regimes defined by Eq. (14), the synchronization either cannot be achieved or the values of ε_n are so high that they cannot be distinguished from no synchronization at all.

5.2. Synchronized states

In the unmodified model, phase locking *i.e.* complete synchronization, related with $\varepsilon_n = 0$ may be achieved only in region of measure zero of the parameter space. When the modifications defined by Eq. (8) and (9) are introduced, the synchronization occurs in wider region of the parameter space. Careful analysis of the results reported in [15] shown that the authors did also use phase reset after “fire”, which hence did not exhibit phase overshoot. An example of a synchronized state is shown in Fig. 3 (a) and (c). The synchrogram shows perfectly horizontal lines. The winding

number is $k = 6$. As discussed in Section 3.2 phase resetting appears to be a necessary condition for existence of phase synchronization in such a system. From the phase diagram Fig. 4 (b) it may be seen that the regions of synchronization and regions of non-synchronization are repeated for each value of k . Typically the synchronization region for a given value of k is located at $M_{k-1} > M > M_k$. Also, there always appears an area in which phase synchronization could not be achieved. In part of the non-synchronized regions there still appears frequency locking but at the border between two area characterized by different winding numbers, the patterns become too complicated to be thoroughly analyzed. An example of such a complicated pattern, shown in Fig. 3 (b) and (d) was analyzed above.

5.3. Symmetry of a variability pattern

After every k beats the fast rotator is kicked by the slow one. This causes a temporary acceleration via phase advance and the corresponding interval is shortened. Similar pattern of activity was shown in vagal modulation of the human heart rate. One difference was that the real vagal activity decelerates the phase [3], which would correspond to negative value of the kick height m^1 . The second difference is such that the interval variability pattern observed in the model shows clear asymmetry as only every k -th beat is directly affected by the slow rotator and after that the rate immediately escapes to the “unperturbed” value. Real pattern of respiratory variability of the heart rate has rather a symmetric sinusoidal shape. In order to obtain such a symmetric pattern the model studied here would have to be modified again. The “lazy” response of the rotator to an external stimulation could be modelled by introduction of inertia. This would require a structural change of the model equations as they describe the system which is already formally overdamped. The impulse characteristics of the force (pulse coupling), which, on the contrary, is not overdamped, seems to stimulate the system too strongly.

An interesting direction in which current work can be followed is to consider another class of systems that exhibit phase synchronization: the relaxation oscillators [6]. These systems are characterized by refraction — temporary insensitivity to external forcing — so the stimulus applied at certain range of phase does not cause phase increment. In consequence the

¹ Such a parameter region was also studied but $m > 0$ was finally selected for current presentation. The results are qualitatively close to each other and $m < 0$ requires careful handling of the “kick” events: when the phase undergoes a stepwise decrease and the final result is below zero. One has to decide whether subsequent evolution of phase should immediately lead to “fire” or not. This problem and a few other technical issues related with the detection of the “fire” event may be avoided by setting $m > 0$ which therefore appeared as a reasonable choice.

system is sensitive to external forcing only in a certain range of phase which seems to facilitate synchronization. Further discussion of the role of diffraction is outside the scope of this work.

6. Conclusions

Using the model of two coupled rotators kicked with delay we were able to reproduce the coupled and non-coupled dynamical regimes described in the literature [15]. We are able to calculate the winding number, the condition for phase synchronization and the phase response function. In contrast to phase resetting published in [12], the fixed point of the phase response function is at least marginally stable. Due to this property the stability region has measure 0 in the parameter space and the Arnol'd tongues do not appear. In order to achieve synchronization it is necessary to introduce phase resetting, which occurs to be a crucial factor for existence of phase synchronization. The respiratory sinus arrhythmia phenomenon is observed in the system. The RSA pattern is, however, clearly asymmetric. In order to obtain the symmetric pattern of RSA observed in experiment some form of inertia should be introduced.

The paper was supported by the Polish Ministry of Science and Higher Education, Grant No. 496/N-COST/2009/0.

REFERENCES

- [1] L.Glass, *Nature* **410**, 277 (2001).
- [2] K. Kuga, I. Yamaguchi, Y. Sugishita *et al.*, *Am. J. Cardiol.* **61**, 361 (1988).
- [3] D.C. Michaels, V.A. Slenter, J. Salata *et al.*, *Am. J. Physiol.* **245**, H1043 (1983).
- [4] J.A. Hirsh, B. Bishop, *Am. J. Physiol.* **241**, H620 (1981).
- [5] M. Barbi, A. Di Garbo, R. Balocchi, *Math. Biosci. Eng.* **4**, 4 (2007).
- [6] J.J. Żebrowski, K. Grudziski, T. Buchner *et al.*, *Chaos* **17**, 015121 (2007).
- [7] T. Buchner, M. Petelczyc, J.J. Żebrowski *et al.*, *Chaos* **19**, 1 (2009).
- [8] P.G. Katona, F. Jih, *J. Appl. Physiol.* **39**, 801 (1975).
- [9] C. Schafer, M.G. Rosenblum, J. Kurths *et al.*, *Nature* **392**, 239 (1998).
- [10] A. Stefanovska, *Nonlinear Phenomena in Complex Systems* **5**, 4 (2002).
- [11] M. McGuinness, Y. Hong, D. Galletly, P. Larsen, *Chaos* **14**, 1 (2004).
- [12] R.E. Mirollo, S.H. Strogatz, *SIAM J. Appl. Math.* **50**, 1645 (1990).
- [13] T. Kuusela, *Phys. Rev.* **E69**, 031916 (2004).
- [14] Y.C. Tzeng, P.D. Larsen, D.C. Galletly, *Am. J. Physiol.* **292**, H1967 (2007).
- [15] D.C. Galletly, P.D. Larsen, *Br. J. Anaesth.* **86**, 777 (2001).

- [16] P.D. Larsen, Y.C. Tzeng, D.C. Galletly, *Auton. Neurosc.* **108**, 45 (2003).
- [17] B.V. Chirikov, *Phys. Rep.* **52**, 263 (1979).
- [18] R. Perez, L. Glass, *Phys. Lett.* **A90**, 441 (1982).
- [19] L. Glass, W-Z. Zeng, *Ann. NY Acad. Sci.* **591**, 316 (1990).
- [20] R. Mrowka, A. Patzak, M. Rosenblum, *Int. J. Bif. Chaos* **10**, 2479 (2000).
- [21] C. Julien, *Cardiovasc. Res.* **70**, 12 (2006).
- [22] S. Daan, D.G. Beersma, A.A. Borbely, *Am. J. Physiol.* **246**, R161 (1984).
- [23] K. Kotani, K. Takamasu, Y. Ashkenazy, H.E. Stanley, Y. Yamamoto, *Phys. Rev.* **E65**, 051923 (2002).
- [24] A.S. Pikovsky, M.G. Rosenblum, J. Kurths, *Int. J. Bif. Chaos* **10**, 2291 (2000).